Journal of Materials Chemistry

Cite this: J. Mater. Chem., 2011, 21, 16339

www.rsc.org/materials

COMMUNICATION

Thinning vertical graphenes, tuning electrical response: from semiconducting to metallic†

Dong Han Seo,[ab] Shailesh Kumar[a] and Kostya (Ken) Ostrikov*[ab]

Received 9th August 2011, Accepted 30th August 2011
DOI: 10.1039/c1jm13835a

A simple, uniquely plasma-enabled and environment-friendly process to reduce the thickness of vertically standing graphenes to only 4–5 graphene layers and arranging them in dense, ultra-large surface area, ultra-open-edge-length, self-organized and interconnected networks is demonstrated. The approach for the ultimate thickness reduction to 1–2 graphene layers is also proposed. The vertical graphene networks are optically transparent and show tunable electric properties from semiconducting to semi-metallic and metallic at room and near-room temperature, thus recovering semi-metallic properties of a single-layer graphene.

Introduction

Dense networks of vertical graphenes hold outstanding promise to dramatically increase the active edge and basal surface areas and achieve the semiconducting properties compared to conventional flat graphene.[1] These abilities are expected to enable unprecedented controls in applications of graphene-based materials in next-generation nanodevices for nano- and optoelectronics, energy conversion, sensing, and biomedicine.[2–9] However, the networks of vertically standing graphenes[10] with tunable electrical properties and chemical reactivity (which is largely determined by the length of open graphitic edges and combined surface areas of basal planes) presently remain a major challenge as the ability to reduce the number of vertical graphene layers remains limited. Indeed, vertically standing carbon nanowalls are typically a few to a few tens of nm thick (thus contain >10 graphene layers)[11] while few-layer graphenes are most commonly achieved as disordered flakes that appear in random places, *e.g.*, by emerging from larger/thicker carbon micro/nanostructures.[12] Plasma-based deposition proved among the most effective approaches to produce such structures, without any catalyst and substrate pre-patterning,[13] similar to inorganic nanostructures.[14–16]

Here we demonstrate a plasma-enabled growth of 4–5 vertical graphene layers on top of reactive edges of catalyst-free, self-organized networks of thicker (~10 graphene layers) vertical graphenes on a Si surface. Effective thinning of vertical graphenes is enhanced by a highly conformal, highly selective plasma-enabled decoration of the top reactive edges with small Cu nanoparticles. The large-area basal planes remain nanoparticle-free thus preserving their original properties. The produced vertical, open-edged, few-layer-graphene structures strictly conform to the top edges of the underlying network of thicker vertical graphene structures (VGSs) with individual segments being up to a few tens of micrometres long and a few micrometres high. We also demonstrate that the hybrid structure not only effectively reduces the electrical resistance of the underlying network by up to 3 orders of magnitude but also enables room-temperature metallic conductivity and recovers semi-metallic graphene properties in an easily achievable temperature range. Our results offer a simple and viable approach towards achieving dense, ultra-large area, ultra-open-edge-length, self-organized networks of vertical graphenes with precisely controlled (ultimately single-layer graphene) thickness and electrical properties easily tunable from semiconducting to semi-metallic and metallic.

Results and discussion

This goal has been achieved in a single vacuum cycle in the integrated plasma nanofabrication system which incorporated magnetron sputtering and inductively coupled plasma enhanced chemical vapour deposition (PECVD, 13.56 MHz, RF power 1.0 kW max) (sketched in Fig. S1†). The p-type Si wafers with thermally oxidized SiO_2 coating of 500 nm thickness were used as substrates for the deposition of VGS-based nanohybrid structures. During the first step (Fig. 1a), networks of thicker vertical graphene structures (termed VGS1 here) were synthesized directly on the substrate surface, without any catalyst, in a gas mixture of 61% CH_4, 31% Ar and 8% H_2. The plasma was generated at the chamber pressure and RF power of 3.0 Pa and 700 W, respectively. The substrates were negatively biased at 60 V DC. No external substrate heating source was used for the deposition. However, the substrate temperature increased up to 450 °C due to the plasma-heating effect[13] during 6 minutes of deposition time. The VGS structures typically reached ~1 to 1.5 μm in heights; the deposition rate was thus 150–250 nm min^{-1}.

Metal–carbon interactions play a crucial role in the catalytic growth of graphitic nanostructures.[17] Moreover, copper has a low affinity to carbon, it almost does not form carbide phases, and Cu atoms are able to form an intermediate bond with carbon atoms *via*

[a]*Plasma Nanoscience Centre Australia (PNCA), CSIRO Materials Science and Engineering, P.O. Box 218, Lindfield, New South Wales, 2070, Australia*
[b]*Plasma Nanoscience @ Complex Systems, School of Physics, University of Sydney, New South Wales, 2006, Australia. E-mail: Kostya.Ostrikov@csiro.au; Fax: +61-2-94137200; Tel: +61-2-94137634*
† Electronic supplementary information (ESI) available. See DOI: 10.1039/c1jm13835a

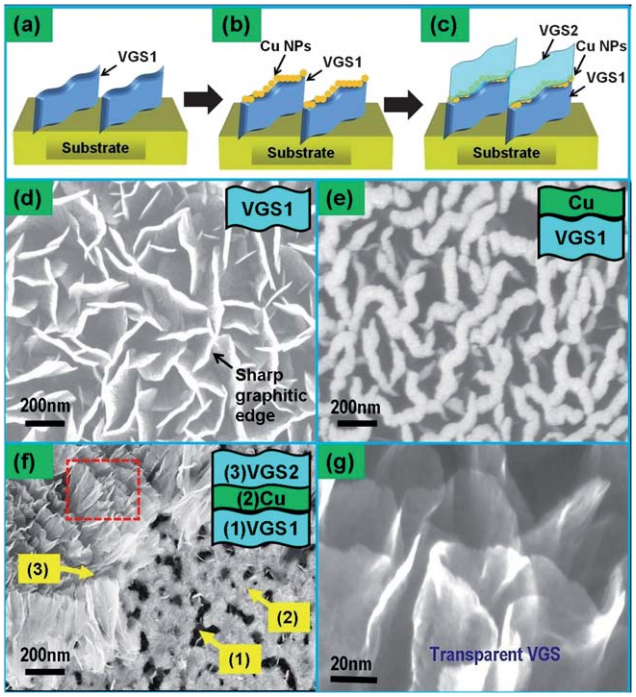

Fig. 1 Schematics show (a) growth of self-organized vertical graphene structures (indicated as VGS1) on a Si substrate with a thin oxide layer, (b) Cu nanoparticles (NPs) deposited only on the edges of VGS1 structures, and (c) vertically and horizontally directed growth of thin, transparent VGSs (indicated as VGS2) on top of Cu NPs decorated VGS1 networks. (d) Top-view SEM image of VGS1 networks as a base layer of the nanohybrid structure. The VGSs feature upright-oriented sharp graphitic edges. (e) Vertical Cu–VGS1 nanohybrid networks; copper NPs are deposited strictly on the sharp graphitic edges of the nanosheets. (f) Tilted cross-sectional SEM image of the scratched portion of the VGS2–Cu–VGS1 nanohybrid networks with labels 1–3 denoting the base VGS1 layer, the Cu NP layer, and the top VGS2 layer, respectively. (g) The high-resolution SEM micrograph reveals that the VGS layer is optically transparent and is much thinner than the VGS1 layer.

charge transfer (π electrons from sp^2-hybridized carbon to 4*s* states of Cu).[18] This ability of copper makes it an efficient catalyst for the growth of graphenes. Therefore, during the second step sketched in Fig. 1b, we have performed a highly selective, conformal deposition of small Cu nanoparticles only on the open reactive edges of the VGSs produced in the first step. For the growth of Cu–VGS1 networks, the VGS1 networks were grown on the substrates at the same conditions as mentioned above. Subsequently, copper nanoparticles were deposited on the VGS1 networks using DC magnetron sputtering at the chamber pressure and power of 4.0 Pa and 100 W, respectively. The deposition of Cu was carried out for 2 minutes (with the deposition rate 50 nm min^{-1}). Finally, we have resumed the PECVD process to grow the second layer of markedly thinner vertical graphene structures (VGS2) on the Cu nanoparticle-decorated graphene edges of the thicker VGS1 base layer as sketched in Fig. 1c.

Fig. 1d shows the top-view scanning electron microscopy (SEM) image of vertically oriented VGS1 networks on the catalyst-free silicon substrate. One can see that most of the VGSs form network connections and also micro-/nanocavities, while some connections remain discontinuous. The growth mechanism of these structures has been reported elsewhere.[12] These VGSs feature sharp graphitic edges[19,20] that are oriented upright from the substrate surface. The electronic states at the sharp edges are higher (hence, the surface energy) compared to the graphitic basal plane, which depends on the arrangement of the carbon atoms forming a zigzag or armchair configuration on the edges.[21] In turn, the higher surface energy on the edges combined with the unique ability of the plasma to charge surfaces and concentrate fluxes of energy and matter near the tips/top edges of high aspect-ratio one- and two-dimensional nanostructures' direct Cu nanoparticle (NP) deposition onto the open edges of VGS1 structures.

Fig. 1e shows copper NPs deposited onto VGS1 networks. We emphasize that copper is deposited *only* on the sharp graphitic edges of the vertical structures rather than on the basal graphitic planes. In this way, a unique self-organized, Cu–VGS1 nanohybrid network is formed. One can also notice that the gaps between some disconnected VGSs within the networks have reduced. Fig. S2† further supports these conclusions. Indeed, from a top-view SEM image in Fig. S2a†, one can see a good degree of conformity of Cu nanoparticles to the two-dimensional maze-like morphology formed by the VGS1 structures. A high-resolution TEM micrograph in Fig. S2b† in turn suggests a reasonably good attachment of Cu nanoparticles to the open edges of VGS1 structures. These Cu nanoparticles can form edge-contact junctions with the VGS due to a soft bonding between graphitic carbon and copper *via* effective charge transfer. The results of energy dispersive X-ray spectroscopy (Fig. S2c†) confirm the expected carbon–copper elemental composition of the Cu–VGS1 nanohybrid structure.

After deposition of the VGS2 layer on the top of the copper-decorated VGS1 network, a VGS2–Cu–VGS1 sandwiched structure is produced. Fig. 1f shows a tilted cross-sectional view of the scratched VGS2–Cu–VGS1 sample. It also shows that only the VGS2 top layer has been removed from the hybrid networks for the subsequent HRTEM analysis. From Fig. 1f and g one can conclude that, in contrast to the VGS1 layer, the VGS2 structures are well interconnected to each other and are also optically transparent.

Further investigations were performed using transmission electron microscopy (TEM). Fig. 2a shows a low-resolution TEM image of a graphene nanosheet directly scratched off from the as-grown VGS1 layer to a TEM grid. The high-resolution (HR) TEM imaging taken at Location 1 of a VGS structure (shown by an arrow mark in Fig. 2a) suggests a typical thickness of approximately 8–10 graphene layers. Fig. 2b confirms that the distance between two graphene layers (0.34 nm) is exactly as expected for graphitic planes. One can notice that these structures have open graphitic edges (as shown by white arrow marks in Fig. 2b), which are highly reactive sites for the Cu NP decoration. The electron diffraction pattern of the vertical graphenes is also shown in the inset of Fig. 2b which clearly shows the 6-fold symmetry diffraction spots. Furthermore, the HR TEM investigation reveals that the VGSs of the top layer of the VGS2–Cu–VGS1 hybrid structure are as thin as only 5 graphene layers, which can be seen in Fig. 2c.

To explain the observed thinning of the graphene sheets in the top layer compared to the bottom one, we note that Cu nanoparticles have been deposited *only* on the (partially) open graphitic edges of the vertical structures rather than on their basal graphitic planes. This deposition is favoured in the open (reactive) areas and leads to the formation of Cu nanoparticles of a typically smaller size than the edge thickness. The sizes of critical nuclei for the formation of vertically

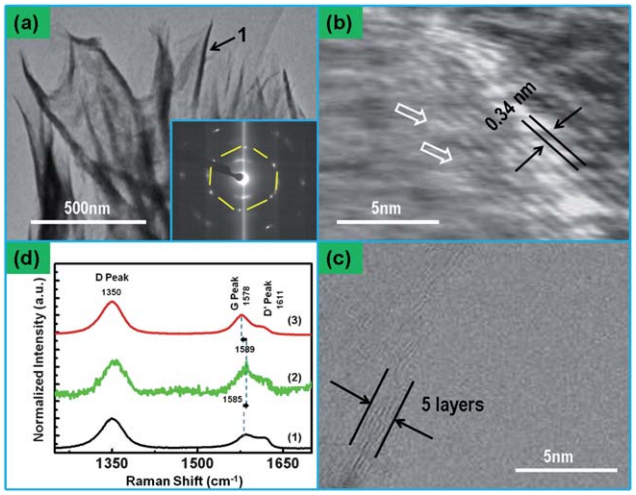

Fig. 2 (a) Low-resolution TEM image of a typical VGS1 structure. (b) HR TEM image taken at location 1 in (a) shows graphene layers; it reveals the presence of many sharp open graphitic edges, as indicated by white arrows. The inset of (b) shows the selected area electron diffraction (SAED) pattern of VGS structures which displays the 6-fold symmetry diffraction spots. (c) HR TEM image of thin VGS2 structures shows only 5 graphene layers. (d) Raman spectra of the VGS1 networks (curve 1), Cu–VGS1 networks (curve 2), and VGS2–Cu–VGS1 networks (curve 3).

aligned nanostructures are usually smaller than the catalyst dimensions, which is quite similar to carbon nanotubes and other nanostructures.[13] This effect, in combination with the ability of the plasma to concentrate fluxes of energy and matter near the tips/top edges of high-aspect-ratio two-dimensional vertically aligned nanostructures, eventually results in the effective thinning of the VGS2 structures compared to the underlying VGS1 network.

Micro-Raman spectroscopy was used to analyse the structural properties of as-grown VGSs after the different fabrication stages of VGS2–Cu–VGS1 hybrid structures (the Raman spectra are shown in Fig. 2d). There are two distinct peaks, namely a graphitic G-peak and a disorder-related D-peak which are located at 1585 and 1350 cm^{-1}, respectively (spectrum 1 in Fig. 2d corresponds to the VGS1 bottom layer). The G-peak is activated due to the C-bond stretching in sp^2-rings, while the D-peak originates due to the presence of many graphitic edges that are abundant in the VGS networks.[22] Therefore, the D-peak is also observed for the Cu–VGS1 (spectrum 2 in Fig. 2d) and VGS2–Cu–VGS1 networks (spectrum 3 in Fig. 2d). The deposition of copper introduces compressive strain in the vertical graphene structures which in turn results in the observed blue shift of the G-peak[23] from 1585 to 1589 cm^{-1} for the Cu–VGS1 networks (see Fig. 2d). Upon deposition of the top layer of the VGS2 structures on top of the Cu–VGS1 networks, one can expect the interplay between the effects of better graphitic ordering and the reduction in compressive stress in the top layer of the VGS2–Cu–VGS1 networks. Therefore, the G-peak is red-shifted to 1578 cm^{-1}. One shoulder peak (D′-peak) also appears at 1611 cm^{-1} which originates from an intra-valley double resonance process.[24]

The temperature-dependent electrical resistance $R(T)$ properties of VGS networks were investigated from room temperature to 4 K using a physical property measurement system (PPMS). The resistance of the VGS1 networks in the first layer of the sandwiched structure was measured to be as high as 700 Ω at room temperature, which then increased as the temperature decreased (as shown in Fig. 3a). This behaviour reveals a pronounced semiconducting nature of the VGS1 networks. From Fig. 3b, one can notice that the resistance drops down below 300 Ω at room temperature for the Cu NPs decorated VGS networks (Cu–VGS1 networks). However, the resistance $R(T)$ curve (Fig. 3b) shows that the Cu–VGS1 nanohybrid structure still behaves as a semiconducting network where the resistance increased up to 500 Ω at lower temperatures.

However, the most dramatic change in the electrical conductivity properties takes place after the second layer of vertical graphenes is deposited. Indeed, the VGS2–Cu–VGS1 networks show the unique transition from metallic to semi-metallic and then to semiconducting behaviour as the temperature decreases. The resistance curve (Fig. 3c) shows that the resistance of the networks decreases as the temperature decreases from room temperature to 200 K ($dR/dT > 0$), which reveals the metallic behaviour of the networks. Between 125 and 200 K, the resistance is almost constant (below 0.5 Ω) and shows a semi-metallic behaviour, similar to a single-layer graphene. However, the network resistance increases as the temperature decreased further below 125 K ($dR/dT < 0$), which reveals the low-temperature semiconducting behaviour. The electrical resistivity measurement results showed a good fit to the Mott's Variable Range Hopping (VRH) model (as shown in the insets of Fig. 3a–c for the corresponding resistance curves of the networks). This fitting reveals that the conduction mechanism in the networks is dominated by the hopping mechanism[25,26] in the semiconducting region.

Let us interpret the observed unique electrical response of the produced networks. The VGS networks have many two-dimensional vertical nanostructures that are interconnected to each other. The points of contact in these interconnections are numerous and therefore introduce defect states in the VGSs.[27] These defect states may trap the carriers thereby limiting their mobility in the VGS networks. Likewise, there are some gaps between the nanosheets in the base-layer networks which in turn create a significant energy barrier for the carrier transport (Fig. 3d). Therefore, the electron conduction mechanism in the networks is dominated by the hopping mechanism in a broad range of temperatures. This is why the VGS1 networks are characterized by a high resistance (~500 Ω). With copper deposition on the sharp edges of graphene nanosheets, the carrier mobility in the individual VGS structures and their contact points with other nanosheets are dominated through the chains of Cu nanoparticles at the edges. Moreover, the gaps between disconnected nanosheets are reduced after Cu NP decoration, as shown in the SEM image, Fig. 1e. These smaller gaps between the copper strips on the nanosheets substantially reduce the energy barrier for the carrier transport, which improves the network conductivity (Fig. 3e). This effect appears to be stronger compared to the effect of junctions between the interconnected VGS structures which provide defect states for carrier conduction thus increasing the network resistance. This explains the observed substantially lower resistance of the Cu–VGS1 networks as compared to the VGS networks.

In the final nanohybrid VGS2–Cu–VGS1 structure, the copper strips on the two adjacent VGS edges in the first layer are further modified during the deposition of the top VGS2 layer. As a result, the copper strip becomes almost continuous between the two VGS edges (Fig. 3f). However, the junctions between interconnected VGS structures provide defect states for carrier conduction, which in turn increases the resistance. Therefore, the probability of the carrier transport from the vertical graphene sheets to the intermediate layer

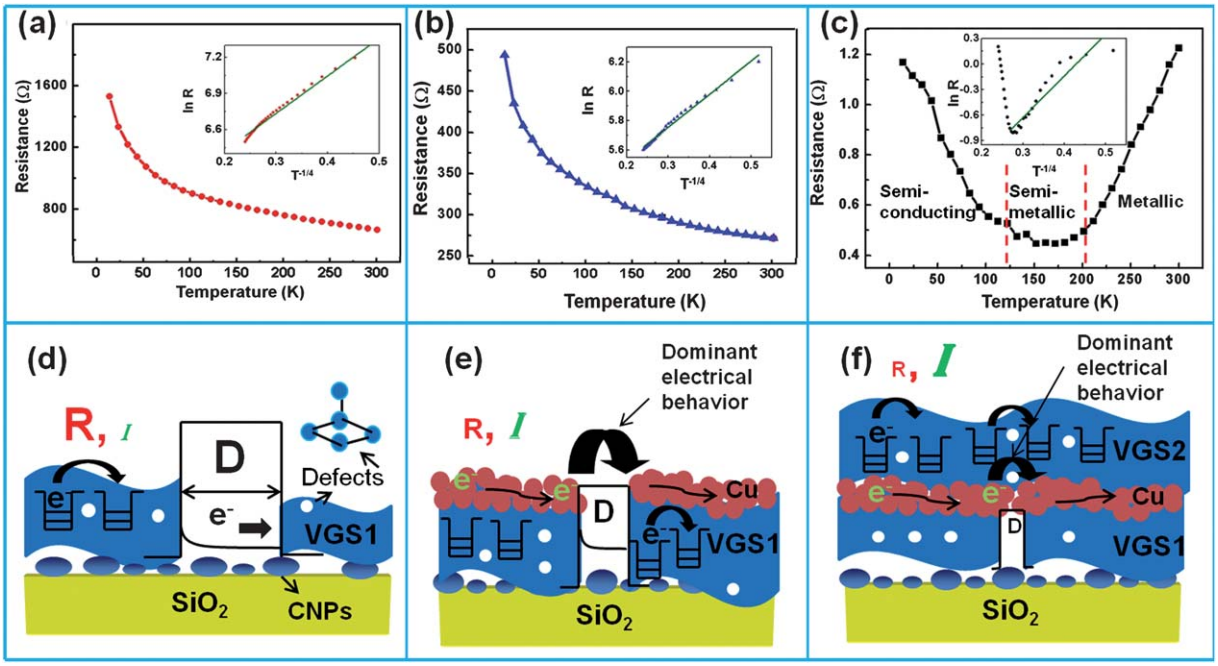

Fig. 3 Temperature-dependent resistance curves and corresponding Mott's plot of the Variable Range Hopping (VRH) model of the VGS1 networks (a), Cu–VGS1 networks (b), and VGS2–Cu–VGS1 networks (c). Schematics of the electron transport mechanisms in the VGS1 networks (d), Cu–VGS1 networks (e), and VGS2–Cu–VGS1 networks (f).

of copper nanoparticles becomes much higher than from one VGS to another. As a result, the resistance of the networks significantly reduced to less than ~2 Ω at room temperature and the VGS2–Cu–VGS1 nanohybrid networks behave as metallic from 200 K to room temperature and above. However, the electron tunnelling in the copper layer is not effective at temperatures lower than 200 K. Consequently, the intrinsic semiconducting properties of the VGS2 layer prevail and one can obtain the switch-over between the metallic and semiconducting properties in the easily accessible temperature range.

Conclusion

This work showed a viable pathway to achieve the presently elusive self-organized vertically standing graphene structures and ultimately reduce their thickness to a single vertical graphene layer. This was achieved in the same vacuum cycle, in a simple, fast, and environment-friendly plasma-based process, which demonstrated: (i) catalyst-free growth of vertical graphenes with a typical thickness of ~10 atomic layers and open reactive edges; (ii) precise, highly conformal decoration of these edges by small Cu nanoparticles leaving the basal graphitic planes intact; and (iii) using these Cu nanoparticles, effective growth of significantly thinner vertically standing graphenes as thin as only 4–5 atomic layers.

Our few-layer graphene structures are optically transparent and conform to the top edges of the underlying network of thicker vertical structures and form an interconnected, self-organized network with unique electrical properties, very large (and clean) surface areas, as well as ultra-long and dense open reactive edges. This unique hybrid structure made it possible not only to dramatically reduce the electrical resistance by up to 3 orders of magnitude but also to demonstrate a switch-over of the electrical properties from semiconducting to metallic, thereby recovering graphene's semi-metallic properties in an easily achievable temperature range.

Acknowledgements

Authors thank Q. J. Cheng for his assistance in TEM imaging. This work was partially supported by the Australian Research Council, CSIRO OCE Postgraduate Scholarship Programme, and CSIRO OCE Science Leadership Programme.

References

1 C. H. Lui, L. Liu, K. F. Mak, G. W. Flynn and T. F. Heinz, *Nature*, 2009, **462**, 339.
2 B. J. Kim, M. S. Kang, V. H. Pham, T. V. Cuong, E. J. Kim, J. S. Chung, S. H. Hur and J. H. Cho, *J. Mater. Chem.*, 2011, **21**, 13068.
3 Y. Ye, L. Gan, L. Dai, H. Meng, F. Wei, Y. Dai, Z. Shi, B. Yu, X. Guo and G. Qin, *J. Mater. Chem.*, 2011, **21**, 11760.
4 M.-Y. Yen, C.-C. Teng, M.-C. Hsiao, P.-I. Liu, W.-P. Chuang, C.-C. M. Ma, C.-K. Hsieh, M.-C. Tsai and C.-H. Tsai, *J. Mater. Chem.*, 2011, **21**, 12880.
5 A. H. Castro Neto, F. Guinea, N. M. R. Peres, K. S. Novoselov and A. K. Geim, *Rev. Mod. Phys.*, 2009, **81**, 109.
6 H. Bi, F. Huang, J. Liang, X. Xie and M. Jiang, *Adv. Mater.*, 2011, **23**, 3202.
7 A. A. Balandin, S. Ghosh, W. Bao, I. Calizo, D. Tewldebrhan, F. Miao and C. N. Lau, *Nano Lett.*, 2008, **8**, 902.
8 Y. Huang, X. Dong, Y. Liu, L.-J. Li and P. Chen, *J. Mater. Chem.*, 2011, **21**, 12358.
9 K. Liu, J.-J. Zhang, F.-F. Cheng, T.-T. Zheng, C. Wang and J.-J. Zhu, *J. Mater. Chem.*, 2011, **21**, 12034.
10 S. Kumar and K. Ostrikov, *Nanoscale*, 2011, DOI: 10.1039/c1nr10860c.
11 K. Tanaka, M. Yoshimura, A. Okamoto and K. Ueda, *Jpn. J. Appl. Phys.*, 2005, **44**, 2074.
12 D. H. Seo, S. Kumar and K. Ostrikov, *Carbon*, 2011, **49**, 4331.
13 K. Ostrikov, *Rev. Mod. Phys.*, 2005, **77**, 489.

14 U. Cvelbar, Z. Chen, M. K. Sunkara and M. Mozetic, *Small*, 2008, **4**, 1610.
15 J. Shieh, F. J. Hou, Y. C. Chen, H. M. Chen, S. P. Yang, C. C. Cheng and H. L. Chen, *Adv. Mater.*, 2010, **22**, 597.
16 J. Zheng, R. Yang, L. Xie, J. Qu, Y. Liu and X. Li, *Adv. Mater.*, 2010, **22**, 1451.
17 F. Banhart, *Nanoscale*, 2009, **1**, 201.
18 C. Mattevi, H. Kim and M. Chhowalla, *Nanoscale*, 2011, **21**, 3324.
19 J. R. Miller, R. A. Outlaw and B. C. Holloway, *Science*, 2010, **329**, 1637.
20 S. Kumar, P. K. Yadav, J. Hamilton and J. McLaughlin, *Diamond Relat. Mater.*, 2009, **18**, 1070.
21 X. Jia, M. Hofmann, V. Meunier, B. G. Sumpter, J. Campos-Delgado, J. M. Romo-Herrera, H. Son, Y.-P. Hsieh, A. Reina, J. Kong, M. Terrones and M. S. Dresselhaus, *Science*, 2009, **323**, 1701.
22 I. Levchenko, O. Volotskova, A. Shashurin, Y. Raitses and M. Keidar, *Carbon*, 2010, **48**, 4556.
23 Z. H. Ni, H. M. Wang, Y. Ma, J. Kasim, Y. H. Wu and Z. X. Shen, *ACS Nano*, 2008, **2**, 2301.
24 L. M. Malard, M. A. Pimenta, G. Dresselhaus and M. S. Dresselhaus, *Phys. Rep.*, 2009, **473**, 51.
25 X. Wang, F. Liu, G. T. S. Andavan, X. Jing, K. Singh, V. R. Yazdanpanah, N. Bruque, R. R. Pandey, R. Lake, M. Ozkan, K. L. Wang and C. S. Ozkan, *Small*, 2006, **2**, 1356.
26 J. Geng, M. D. R. Thomas, D. S. Shephard and B. F. G. Johnson, *Chem. Commun.*, 2005, 1895–1897.
27 E. Yoo and H. Zhou, *ACS Nano*, 2011, **5**, 3020.